Astron. Astrophys. 346, 713–720 (1999)

ASTRONOMY AND ASTROPHYSICS

Comptonization of photons in advection dominated accretion flows

A Monte Carlo approach

A. Kurpiewski and M. Jaroszyński

Warsaw University Observatory, Al. Ujazdowskie 4, PL-00-478 Warsaw, Poland

Received 18 February 1999 / Accepted 30 March 1999

Abstract. We study the formation of the spectra in Advection Dominated Accretion Flows (ADAFs) around Kerr black holes. We use a Monte Carlo approach and fully general relativistic treatment to follow the paths of individual photons and model their scattering with mildly relativistic, thermal electrons of the two temperature plasma present in the flow. We are mostly interested in the dependence of the spectra on the black hole angular momentum, and we find that the influence of the black hole rotation rate on the flow structure has an impact on the resulting spectra. The flows around the fast rotating holes produce relatively harder spectra. This property of the models should be taken into account when modeling the individual sources and the population of inefficiently accreting black holes in the Universe.

Key words: accretion, accretion disks – black hole physics – radiation mechanisms: non-thermal – radiation mechanisms: thermal

1. Introduction

The Advection Dominated Accretion Flows (ADAFs) have been reviewed by a number of authors, most recently by Narayan et al. (1998), Kato et al. (1998), and Lasota (1998). The ADAFs represent a class of optically thin solutions of the accretion flow, which radiate so inefficiently, that almost all the heat dissipated inside the fluid is subsequently advected toward the black hole horizon. Since the cooling of matter is negligible, the equations of fluid dynamics are independent of the equations describing the emission, absorption and scattering of radiation. This allows one to address these two topics separately. In this paper we are concerned mostly with the radiation processes inside the flow.

The fully relativistic dynamics of ADAFs has been described and some solutions have been obtained in Lasota (1994), Abramowicz et al. (1996, hereafter ACGL), Abramowicz et al. (1997), Peitz & Appl (1997), Jaroszyński & Kurpiewski (1997, hereafter Paper I), Gammie & Popham (1998), and Popham & Gammie (1998). The most extensive survey of the parameter space is probably presented by Popham & Gammie (1998), where the dependence of the flow on the black hole spin a, the viscosity parameter α, the gas adiabatic index and on the advection parameter f (where $f = 1$ means fully advective flow without any cooling) is investigated. This work shows rather strong dependence of the flow characteristics on parameters mentioned, especially on the black hole spin. The dependence on advection parameter is also substantial, but for a narrow range of f, which can represent flows with negligible cooling ($0.9 \leq f \leq 1$) one can use the $f = 1$ solutions. Similarly, the solutions depend strongly on the viscosity parameter α, but for the limited range of this parameter ($\alpha \geq 0.01$), which is more physically relevant (Balbus et al. 1995), the differences between the solutions are not dramatic, in particular the topology of the isobars is the same.

In our calculations we use the solutions of the equations describing the flow dynamics presented in Paper I. All our models use $f = 1$ and $\alpha = 0.1$. Both values are representative of the physically relevant ADAFs. The black hole spin, we consider, is limited to the three values ($a = 0$, 0.5, and 0.9).

The main purpose of this paper is a self-consistent treatment of photon Comptonization in a two temperature plasma of an ADAF solution. To do so we need a 3D distribution of matter density, velocity and temperature, while the standard solutions give only the vertically averaged quantities as measured at the equator. At this point it is important to choose the relevant method of vertical averaging and we follow Abramowicz et al. (1997), Quataert & Narayan (1998) and Paper I in choosing averaging on spheres (and not on cylinders). In this approach the matter distribution in space is limited by the centrifugal forces barrier and does not resemble the infinite isothermal atmosphere, obtained in the alternative approach.

We calculate the spectrum of photons leaving the flow. The photons originate in bremsstrahlung and thermal synchrotron processes, which can be described locally. The scattering (if any) can take place at any point of the photon trajectory inside matter distribution and is nonlocal. We simulate this process using Monte Carlo approach. Our simulation of photon Comptonization is quite standard, but the flow, where the processes take place is rather complicated. Since the optical depth for scattering is low, a photon can travel to a distant part of the fluid before undergoing any interaction. The relative motion of the fluid elements, where consecutive interactions of photons with matter take place, can be substantial. Also, the photons traveling in the densest parts of the flow, near the horizon, can be deflected

by the gravitational field. This and other relativistic effects in photon motion are included in our study.

The main aim of our investigation is the self-consistent treatment of Comptonization. Most non-analytical thermal Comptonization models use iterative methods of solving the kinetic equations (e.g. Poutanen & Svensson 1996). This method has been adopted by Narayan et al. (1997) to calculate the spectrum of soft X-ray transient source V404 Cyg in which, they believe, ADAF exists. In our calculations we use Monte Carlo method which has been described in most detail by Pozdnyakov et al. (1977) and Górecki & Wilczewski (1984). This method allows us to follow only one photon at a time and we are not able to take into account the creation of e^+e^- pairs. However as Björnsson et al. (1996) and Kusunose & Mineshige (1996) showed, the role of e^+e^- pairs in ADAFs is not significant.

In the next section we briefly characterize the model of ADAF. The method of Monte Carlo Comptonization is presented in Sect. 3. In Sect. 4 we present the results of calculations, showing the ADAFs spectra. The discussion and conclusions follow in the last section.

2. The 3D description of the fluid

2.1. The accretion flow

We investigate the stationary flow of matter and the propagation of light in the gravitational field of a rotating Kerr black hole using the Boyer-Lindquist coordinates t, ϕ, r, θ and the metric components $g_{ab}(r,\theta)$ as given by Bardeen (1973). We follow the $(-,+,+,+)$ signature convention. We use geometrical units, so the speed of light $c \equiv 1$ and the mass of the hole $M \equiv 1$. The Kerr parameter a ($0 \leq a < 1$) gives the black hole angular momentum in geometrical units. We use the Einstein summation convention, where needed, and a semicolon for the covariant derivative. The normalization of four velocity with the chosen metric signature reads $u^a u_a = -1$.

The system of equations we use follows in general ACGL. Since we are neglecting the cooling processes at this stage, and treat the accretion flow in the disk approximation, two components of velocity and the speed of sound $c_{\rm S}$ given as functions of radius, fully describe the dynamics. We use the angular velocity Ω and the physical radial velocity V as measured by locally nonrotating observers as main kinematic variables (compare ACGL). After the *vertical averaging* the velocity perpendicular to the equatorial plane is neglected ($u^\theta \equiv 0$) and other components of the four velocity are given as:

$$u^t = \frac{1}{\sqrt{1-V^2}\sqrt{-g_{tt}-2\Omega g_{t\phi}-\Omega^2 g_{\phi\phi}}} \tag{1}$$

$$u^\phi = \Omega u^t \tag{2}$$

$$u^r = \frac{1}{\sqrt{g_{rr}}}\frac{V}{\sqrt{1-V^2}}\,. \tag{3}$$

The above velocity components have to be known only at the equatorial plane and its close vicinity if one needs to obtain a system of equations describing an ADAF in the slim disk approximation (Abramowicz et al. 1988). To describe the matter distribution in space (also far from the equatorial plane) one has to introduce further specifications of the velocity and angular momentum distribution, since only the averaged values enter the equations. We assume that the poloidal velocity component (u^θ) is absent and that the radial velocity component V depends on the radius only:

$$V = V(r) \quad u^\theta \equiv 0 \tag{4}$$

(The BL velocity component u^r depends on θ through g_{rr} - compare Eq. 3)

The choice of angular momentum distribution is less obvious. Close to the horizon, where the velocities are highest and possible kinematic effects most important, the specific angular momentum $\ell \equiv -u_\phi/u_t$ is approximately constant (Paper I, ACGL, Peitz & Appl, 1997). We assume ℓ to be exactly constant on spheres:

$$\ell = \ell(r) \tag{5}$$

Since the metric components do depend on θ the angular velocity is not constant on spheres:

$$\Omega = \frac{g^{\phi t}u_t + g^{\phi\phi}u_\phi}{g^{tt}u_t + g^{t\phi}u_\phi} = \frac{g^{\phi t} - \ell g^{\phi\phi}}{g^{tt} - \ell g^{t\phi}} \tag{6}$$

The other kinematic quantities are given as:

$$u_t = \frac{1}{\sqrt{1-V^2}\sqrt{-g^{tt}+2\ell g^{t\phi}-\ell^2 g^{\phi\phi}}} \tag{7}$$

$$u_\phi = -\ell u_t \tag{8}$$

We assume that the accreting plasma contains small scale, isotropically tangled magnetic field resulting from magnetohydrodynamical instability (Balbus et al. 1995). Hence we write the total pressure as

$$p = p_{\rm g} + p_{\rm m} \;\; p_{\rm g} = \beta p \;\; p_{\rm m} \equiv \frac{B^2}{8\pi} = (1-\beta)p \tag{9}$$

where $p_{\rm g}$ is the gas pressure, $p_{\rm m}$ – the magnetic pressure, B – the magnetic field, and β is a constant parameter. The pressure, the rest mass density ρ_0 and the sound velocity $c_{\rm S}$ are related:

$$p = \rho_0 c_{\rm S}^2 \tag{10}$$

In our calculations we use a two temperature plasma with a small amount of magnetic field to represent the matter properties. Thus the ion pressure dominates, the gas is non-relativistic and the specific enthalpy μ is given as:

$$\mu \equiv \frac{\epsilon + p}{\rho_0} = 1 + \frac{5}{2}c_{\rm S}^2 \tag{11}$$

where ϵ is the total (rest mass plus thermal) energy density.

In the ADAF set of equations only the vertically averaged sound speed is used. It is in spirit of our approximations to postulate:

$$c_{\rm S} = c_{\rm S}(r) \tag{12}$$

which means that the gas is isothermal on spheres. The electron temperature $T_{\rm e}$ is much lower than the ion temperature, so its influence on the equation of state and the structure of the flow can be neglected.

Our detailed (but approximate) description of the fluid kinematics makes it possible to find the density dependence on the angular coordinate θ. The set of equations describing ADAF contains viscosity terms, which are included in the energy equation, but neglected in the mechanical equilibrium equations (ACGL, Peitz & Appl 1997, Paper I). Thus it is sufficient to use the ideal fluid energy momentum tensor:

$$T^a_b = (\epsilon + p)u^a u_b + p\delta^a_b \tag{13}$$

The θ conservation equation, $T^a_{\theta;a} = 0$ reads:

$$u^a u_{\theta;a} = \frac{-p_{,\theta}}{\epsilon + p} \tag{14}$$

After some algebra we obtain:

$$\frac{1}{1-V^2}(\ln u_t)_{,\theta} - \frac{1}{2}\frac{V^2}{1-V^2}(ln(r^2 + a^2\cos^2\theta))_{,\theta} = -\frac{c_{\rm S}^2}{\mu}(\ln \rho_0)_{,\theta} \tag{15}$$

Since V does not depend on θ, the LHS of the equation is a full gradient of a quantity which can be called a potential ψ. This implies the solution for the density:

$$\rho_0(\theta) = \rho_{0,\rm eq} \exp\left(-\frac{\mu(\psi(\theta) - \psi_{\rm eq})}{c_{\rm S}^2}\right) \tag{16}$$

where the $\rho_{0,\rm eq}, \psi_{\rm eq}$ denote the values measured at the equatorial plane.

The constant sound speed on the spheres may suggest that the exponential atmosphere never ends. For the rotating configuration there is, however, an infinite potential barrier close to the rotation axis, where $u_t \to \infty$ and $\rho_0 \to 0$. Thus the vicinity of the rotation axis is empty and the density falls steeply down near this region. In this respect the ADAF solutions are similar to the so called thick accretion disks (Abramowicz et al. 1978). Both have empty funnels around their rotation axes.

The mass flow through the $r = const$ surface can be calculated as:

$$\dot{M} = -\int_0^\pi {\rm d}\theta{\rm d}\phi\sqrt{-g}\rho_0(\theta)u^r \tag{17}$$

$$\equiv 2\pi\sqrt{\frac{V^2}{1-V^2}}\int_0^\pi {\rm d}\theta\sqrt{(g_{t\phi}^2 - g_{tt}g_{\phi\phi})g_{\theta\theta}}\rho_0(\theta) \tag{18}$$

Combining the last equation and the formula for the θ dependence of the density we obtain the equatorial value of the density.

2.2. Two temperature plasma

While modeling the dynamics of ADAF we neglect the heat transfer and all the radiation processes, assuming that only a small part of the total energy generated by viscous processes can be affected by them. Now we are going to model the radiation processes.

We assume that the whole energy dissipated is transferred to the ions. The ions heat the electrons via Coulomb collisions and the electrons lose their energy by the synchrotron, bremsstrahlung and inverse Compton cooling processes. In the ADAFs thermalization time-scale greatly exceeds the dynamical time-scale and the plasma remains two temperature. We find the electron and ion temperatures, $T_{\rm e}(r,\theta)$ and $T_{\rm i}(r,\theta)$, self-consistently using the equation of state

$$p_{\rm g} = \beta p = \frac{\rho k T_{\rm i}}{\mu_{\rm i} m_{\rm H}} + \frac{\rho k T_{\rm e}}{\mu_{\rm e} m_{\rm H}} \tag{19}$$

where $\mu_{\rm i} = 1.29$ and $\mu_{\rm e} = 1.18$ are effective molecular weights of the ions and electrons, and the condition of thermal equilibrium applied locally

$$q^+ = q^-_{\rm br} + q^-_{\rm br,C} + q^-_{\rm S} + q^-_{\rm S,C} \tag{20}$$

where q^+ is the rate of Coulomb heating of electrons by ions (e.g. Mahadevan 1997), $q^-_{\rm S}$ and $q^-_{\rm br}$ are the synchrotron and bremsstrahlung cooling rates, and $q^-_{\rm S,C}$ and $q^-_{\rm br,C}$ are the Compton cooling rate of synchrotron and bremsstrahlung photons, respectively.

The calculation of the synchrotron cooling rate is somewhat complicated because the optical depth to absorption (Self Synchrotron Absorption) for majority of the synchrotron photons is high. In our approach we assume that a photon can either escape from the medium carrying out its energy and taking part in cooling process, or be absorbed very close to the point of its original emission and not contributing to the cooling. In reality all photons carry energy and some are absorbed far from the emission point transferring energy to distant portions of the fluid. Our assumption neglects the heat transport between different volume elements, but makes calculations doable.

To find the probability of a photon escape from given location we follow $N \sim 10^2$ rays with directions randomly chosen at the frame comoving with the fluid. The optical depth along a ray measured at the frequency ν is

$$\tau_\nu = \int_0^{l_\infty} \frac{\epsilon_{\rm S}(\nu)}{4\pi B_{T_{\rm e}}(\nu)}{\rm d}l \tag{21}$$

where $\epsilon_{\rm S}$ is the synchrotron emissivity, $B_{T_{\rm e}}$ is the Planck function corresponding to the electron temperature $T_{\rm e}$, and the integration is over the proper distance, l_∞ corresponding to the point on the fluid boundary. Since the integrand in the above formula is the function of the electron temperature we must assume the approximate distribution of the electron temperature in the ADAF. As a first approximation we use our results from Paper I based on the approach of Narayan & Yi 1994. Averaging one gets the probability of escape:

$${\rm e}^{-\tau_\nu} = \frac{1}{N}\sum_{i=1}^{N} {\rm e}^{-\tau_\nu^{(i)}} \tag{22}$$

Since we assume that cooling is provided only by the escaping photons, we have:

$$q_{\rm S}^{-} = \int_0^\infty \epsilon_{\rm S}(\nu)\, {\rm e}^{-\tau_\nu}\, {\rm d}\nu \tag{23}$$

for the synchrotron cooling. We adopt the expressions for synchrotron emissivity from Pacholczyk (1970) and Mahadevan et al. (1996).

For the bremsstrahlung cooling the solution is straightforward. The absorption of low frequency bremsstrahlung photons has no practical meaning, so we adopt their frequency integrated emission as cooling rate

$$q_{\rm br}^{-} = \int_0^\infty \epsilon_{\rm br}(\nu)\, {\rm d}\nu \tag{24}$$

We take the expression for bremsstrahlung cooling rate from Stepney & Guilbert (1983).

Finally we take the cooling by Comptonization of both synchrotron and bremsstrahlung photons using the formulae of Esin et al. (1996). The mean optical depth to Compton scattering is calculated in the same manner as above. Solving the Eqs. 19 and 20 we get the electron temperature and the ion temperature.

2.3. Spectra neglecting comptonization

As a by-product of the calculations of the previous subsections one can obtain the spectrum of the model, which would be valid if the Comptonization were unimportant. For sufficiently low frequencies a photon is rather absorbed than scattered, so both approaches, neglecting and including Comptonization, should give similar results in this regime. This gives a chance of a self check of the simulations.

Calculation of many rays sent from a given fluid element can also be used to find the contribution of this element to the total luminosity of the configuration as seen by a distant observer. If the frequency $\nu_{\rm em}$ and the direction of a photon in the fluid frame is known, its frequency in the Boyer-Lindquist coordinate frame $\nu_{\rm obs}$ can be calculated and this is the frequency that would be measured by a distant observer, unless the photon goes under the horizon. For photons going to infinity the redshift factor can be defined:

$$1 + z = \frac{\nu_{\rm em}}{\nu_{\rm obs}} \tag{25}$$

Distant observers measure photon energies divided by the factor $(1 + z)$. Also the time interval between the detection of two signals is the interval between their sending multiplied by $(1 + z)$. Thus the contribution to the total luminosity from the fluid element of the volume ΔV, measured by distant observers in their frequency interval $\Delta\nu_{\rm obs}$ is given as:

$$L_(\nu_{\rm obs})\Delta\nu_{\rm obs} = \frac{1}{N}\sum_{i=1}^{N} \frac{\epsilon(\nu_{\rm em})\Delta\nu_{\rm em}\, {\rm e}^{-\tau^{(i)}_{\nu_{\rm em}}}}{(1+z_i)^2}\, \Delta V \tag{26}$$

where for the i-th ray:

$$\nu_{\rm em} = \nu_{\rm obs}(1+z_i)\ \ \Delta\nu_{\rm em} = \Delta\nu_{\rm obs}(1+z_i) \tag{27}$$

The summation is limited to rays which reach infinity. Integration over the volume of the fluid gives the total luminosity of the model.

The emission from the configuration is not isotropic, so the observers at different position angles measure a different flux of radiation. The luminosity calculated above is in fact an average of luminosities assigned to the disk by observers uniformly distributed on a sphere around the object. One can also find the average luminosity that would be measured by observers from a limited solid angle $\Delta\Omega$. To do so it is sufficient to neglect in the summation all the rays which do not enter the region of interest and multiply the result by the correction factor $4\pi/\Delta\Omega$.

2.4. Spatial distribution of the photon emissivity

In the Monte Carlo simulations we follow individual photons as they travel through the fluid undergoing consecutive scatterings. We have to know what is the distribution of the points of emission of the photons. We divide the flow into several spherical layers. The radius in the middle of the layer numbered j is r_j. Each layer is then subdivided into annuli of limited range in the polar angle θ between fluid boundaries $\theta_{\rm min}(r_j)$ and $\pi - \theta_{\rm min}(r_j)$. The angular coordinate at the middle of the annulus numbered jk is θ_{jk}. One can assume that all fluid parameters are almost uniform inside each annulus, and take their values at (r_j, θ_{jk}) as representative. Using similar arguments as in the previous subsection we calculate the rate of photon emission from the region numbered jk of the volume ΔV_{jk}:

$$\dot{\mathcal{N}}_{jk} = \frac{\Delta V_{jk}}{N}\sum_{i=1}^{N}\int_0^\infty \frac{\epsilon(\nu_{\rm em})\, {\rm e}^{-\tau^{(i)}_{\nu_{\rm em}}}\, {\rm d}\nu_{\rm em}}{h\nu_{\rm em}(1+z_i)} \tag{28}$$

We adopt the expressions for synchrotron cooling from Pacholczyk (1970) and Mahadevan et al. (1996), and for bremsstrahlung cooling from Svensson (1982) [and references therein]. The cooling rates are functions of the electron temperature, the number density of ions and electrons and the magnetic field density (synchrotron radiation) and hence they are functions of r and θ. We take $\epsilon = \epsilon(r_j, \theta_{jk})$. The expression under the integral is regular at low frequencies despite the presence of $\nu_{\rm em}$ in the denominator because $\tau^{(i)}_{\rm em} \to \infty$ when $\nu_{\rm em} \to 0$. The redshift factor in the denominator takes care of the difference between clock rates in the fluid frame and at infinity.

3. The comptonization

We follow the method of Comptonization described by Górecki & Wilczewski (1984).

3.1. Basic concepts

The differential cross section for Compton scattering is given by the following formula (Akhiezer & Berestetski 1965):

$$\frac{{\rm d}\sigma}{{\rm d}\Omega'} = \frac{r_0^2}{2\gamma^2} X(1 - \boldsymbol{v\Omega}/c)^{-2}\left(\frac{h\nu'}{h\nu}\right)^2 \tag{29}$$

where $h\nu$, $\mathbf{\Omega}$, $h\nu'$ and $\mathbf{\Omega}'$ are respectively the energy and the direction of the photon before and after the scattering, $\boldsymbol{v}$ is the velocity of the electron, γ is the Lorentz factor and r_0 is the classical electron radius. The symbol X denotes the invariant part of the cross section:

$$X = \frac{x}{x'} + \frac{x'}{x} + 4\left(\frac{1}{x} - \frac{1}{x'}\right) + 4\left(\frac{1}{x} - \frac{1}{x'}\right)^2 \tag{30}$$

where

$$\frac{x}{2} = \frac{h\nu}{mc^2}\gamma(1 - \boldsymbol{v}\mathbf{\Omega}/c)\ ,\ \frac{x'}{2} = \frac{h\nu'}{mc^2}\gamma(1 - \boldsymbol{v}\mathbf{\Omega}'/c) \tag{31}$$

are the energies of the incoming photon and of the scattered photon, respectively, expressed in units of mc^2 in the reference frame of the electron. The energies $h\nu$ and $h\nu'$ are related by the Compton formula

$$h\nu' = \frac{h\nu(1 - \boldsymbol{v}\mathbf{\Omega}/c)}{1 - \boldsymbol{v}\mathbf{\Omega}'/c + \frac{h\nu}{\gamma mc^2}(1 - \mathbf{\Omega}\mathbf{\Omega}')} \tag{32}$$

We use the total Compton cross section which is given by (Berestetski et al. 1972)

$$\sigma(x) = \\ = 2\pi r_0^2 \tfrac{1}{x}\left[\left(1 - \tfrac{4}{x} - \tfrac{8}{x^2}\right) ln(1+x) + \tfrac{1}{2} + \tfrac{8}{x} - \tfrac{1}{2(1+x)^2}\right] \tag{33}$$

The basic concept of this method is to follow the photon trajectory from the moment of emission until the photon leaves the flow. The probability that a photon leaves the flow without scattering is

$$P_i = exp\left\{-\int_{\boldsymbol{r}_i}^{\boldsymbol{r}_\infty} n_e \langle\sigma\rangle \mathrm{d}l\right\} \tag{34}$$

where the integral is taken along the photon trajectory from the point of the last (i-th) scattering to the boundary of the flow $\boldsymbol{r}_\infty$, $n_e = \int n_e(\boldsymbol{v})\mathrm{d}^3v$ is the electron density, $n_e(\boldsymbol{v})$ is the electron velocity distribution, and

$$\langle\sigma\rangle = \frac{1}{n_e}\int n_e(\boldsymbol{v})(1 - \boldsymbol{v}\mathbf{\Omega}/c)\sigma(x)\mathrm{d}^3v \tag{35}$$

is a mean cross section averaged over the electron velocity distribution. $n_e(\boldsymbol{v})$.

The probability P_i enables us to find the statistical weights of the number of photons leaving the flow without scattering (and thus contributing to the emerging spectrum) and the photons which remain in the flow and undergo the next ($[i+1]$-th) scattering. These weights are given by $w_i P_i$ and $w_{i+1} = w_i(1-P_i)$, respectively, where $i = 0, 1, 2, 3, ...$ is the index denoting the succeeding scatterings. We assume $w_0 = 1$. We follow the trajectory of the photon until w becomes less than a certain minimal value $w_{\min}$. Since ADAFs are optically thin (in our model the Thomson optical depth is about 0.1 in equatorial directions) the mean number of scatterings is 4–5 for $w_{\min} = 10^{-7}$.

3.2. Generating the random variables

The random variables are generated from the probability distributions using Monte Carlo methods: the inversion of the cumulative distribution function or von Neumann's rejection technique. Multi-dimensional distributions are modeled using the conditional probability distributions.

(i) At first we generate the position vector at which the photon is initially emitted. According to our approximation this position is uniformly distributed in space within each of the annuli jk. The probability that a photon is emitted from a region of the given number jk is:

$$f_{jk} = \frac{\dot{\mathcal{N}}_{jk}}{\sum_{j',k'}\dot{\mathcal{N}}_{j'k'}} \tag{36}$$

where $\dot{\mathcal{N}}_{jk}$ are given in Eq. 28. In Eq. 28 we take into account the optical depth due to the absorption, so the number of the low frequency photons we use in the simulation is the expected number of the photons which have a chance of escape. The absorption does not have to be considered on the further photon trajectory. (After a scattering with relativistic electrons a photon gains so much energy that the possibility of its absorption can be neglected. The probability of absorption on the original trajectory is included in Eq. 28.)

(ii) As the position of input photon is determined we can generate the initial energy of the photon $h\nu_0$ using a probability distribution specified by the photon spectrum of synchrotron or bremsstrahlung emission

$$f_{jk}(\nu) = \frac{n_\nu(r_j, \theta_{jk})}{\int_0^\infty n_\nu(r_j, \theta_{jk})\mathrm{d}\nu} \tag{37}$$

where $n_\nu(r_j, \theta_{jk})[Hz^{-1}cm^{-3}s^{-1}]$ is the photon spectrum approximated by formulae of Pacholczyk (1970) and Mahadevan et al. (1996) for synchrotron emission or Svensson (1982) for bremsstrahlung emission. The photon spectrum is determined from the energy spectrum by dividing the last one by $h\nu$.

(iii) We assume that the emission of input photons is isotropic. Hence the direction of the photon in a comoving Cartesian coordinate frame $\mathbf{\Omega}$= $(\sin\Theta\cos\Phi, \sin\Theta\sin\Phi, \cos\Theta)$ is generated from uniform distributions in the ranges $\cos\Theta \in [-1; 1]$ and $\Phi \in [0; 2\pi]$.

In this way we determine the set of parameters $\{\boldsymbol{r}_0,\ h\nu_0,\ \mathbf{\Omega}_0,\ w_0 = 1\}$ describing the initial point of the trajectory of the photons beam. We calculate the next points of the trajectory, i.e. $\{\boldsymbol{r}_{i+1}, h\nu_{i+1}, \mathbf{\Omega}_{i+1}, w_{i+1}\}$ ($i = 0, 1, 2, 3, ...$) until $w = w_{min}$. The way of computing the weights w_i is described in Sect. 3.1. Below we present the way of computing the position, energy and direction of a photon after following scatterings.

(iv) The position $\boldsymbol{r}_{i+1}$ is found on the photon trajectory at the proper distance l from the starting point $\boldsymbol{r}_i$, from the probability distribution:

$$f(l) = \frac{\mathrm{e}^{-\tau(l)}\frac{\mathrm{d}\tau(l)}{\mathrm{d}l}}{\int_0^{l_\infty} e^{-\tau(l)}\frac{\mathrm{d}\tau(l)}{\mathrm{d}l}\mathrm{d}l} \tag{38}$$

where

$$\tau(l) = \int_0^l n_{\rm e}\langle\sigma\rangle {\rm d}l \tag{39}$$

(v) The two remaining parameters $h\nu_{i+1}$ and $\mathbf{\Omega}_{i+1}$ of the $(i+1)-th$ point of the photon trajectory are obtained by simulating the scattering of the photon of energy $h\nu_i$ and direction $\mathbf{\Omega}_i$ by an electron with velocity $\boldsymbol{v}$. To describe the probability distribution of this scattering we use the differential cross section (1):

$$f_{(h\nu_i,\mathbf{\Omega}_i)}(\boldsymbol{v},\mathbf{\Omega}_{i+1}) = = \frac{n(\boldsymbol{v})(1-\boldsymbol{v}\mathbf{\Omega}_i/c)\frac{{\rm d}\sigma}{{\rm d}\Omega_{i+1}}}{\iint n(\boldsymbol{v})(1-\boldsymbol{v}\mathbf{\Omega}_i/c)\frac{{\rm d}\sigma}{{\rm d}\Omega'}{\rm d}^3\Omega'{\rm d}^3\boldsymbol{v}} \tag{40}$$

We model the multi-dimensional probability distribution (13) as a product of the probability distribution of $\boldsymbol{v}$ and the conditional probability distribution of $\mathbf{\Omega}_{i+1}$

$$f_{(h\nu_i,\mathbf{\Omega}_i)}(\boldsymbol{v},\mathbf{\Omega}_{i+1}) = f_1(\boldsymbol{v})f_2(\mathbf{\Omega}_{i+1}|\boldsymbol{v}) \tag{41}$$

where

$$f_1(\boldsymbol{v}) = \frac{n(\boldsymbol{v})}{n_e}(1-\boldsymbol{v}\mathbf{\Omega}_i/c)\frac{\sigma(x)}{\langle\sigma\rangle} \tag{42}$$

and

$$f_2(\mathbf{\Omega}_{i+1}|\boldsymbol{v}) = \frac{1}{\sigma(x)}\frac{{\rm d}\sigma}{{\rm d}\Omega_{i+1}} \tag{43}$$

We generate the velocity $\boldsymbol{v}$ from Eq. 42 and then the direction $\mathbf{\Omega}_{i+1}$ from Eq. 43. Having $\mathbf{\Omega}_{i+1}$, the energy of the scattered photon $h\nu_{i+1}$ can be obtained from the Compton formula (32). The detailed description of the method of modeling the probability distributions $f_1(\boldsymbol{v})$ and $f_2(\mathbf{\Omega}_{i+1}|\boldsymbol{v})$ can be found in Górecki & Wilczewski (1984).

4. Results

We have performed trial calculations of the ADAFs spectra employing the method described. We use the models of ADAFs from Paper I. For the black hole mass, accretion rate and parameter β we use the parameters of Lasota et al. (1996), $M_{\rm BH} = 3.6\times10^7 M_\odot$, $\dot{m} = 0.016$, $\beta = 0.95$, which they apply in the modeling of NGC 4258. We do not, however, attach cold, thin disks at large radii to our ADAF solutions. In Fig. 1 we show the input spectra of synchrotron and bremsstrahlung photons as well as the resulting Comptonized spectrum of the disk around $a = 0.9$ black hole. All the spectra in this and other diagrams are shown as $\lg(\nu)$ versus $\lg(\nu F_\nu)$ plots. For the synchrotron input the results are based on calculations including 10^6 input photons and following more than 5×10^6 branches of photon trajectories. The Comptonization plays a less important role in the case of bremsstrahlung radiation, so we use ~ 10 times fewer photon trajectories to obtain the spectra in this case. Since the Comptonization preserves the photon number, we normalize the spectra using Eq. 28 with either synchrotron or bremsstrahlung emissivity under the integral to obtain the relative numbers of seed photons of each kind.

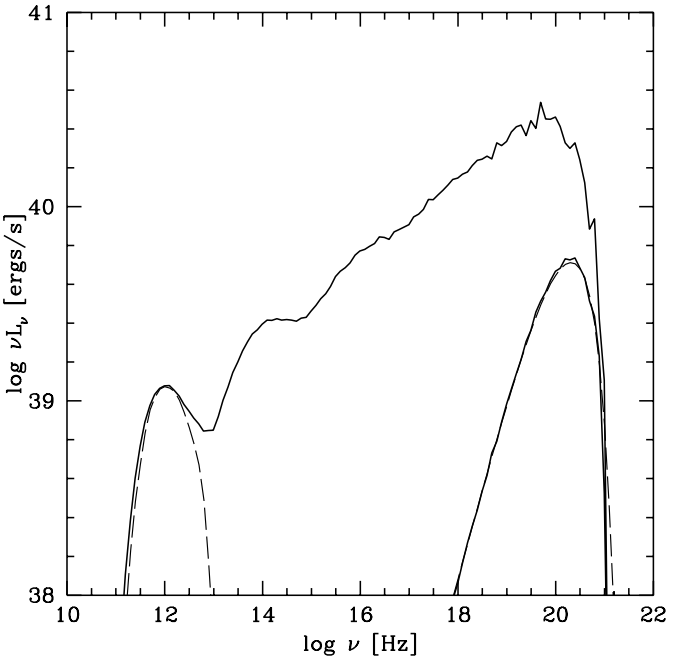

Fig. 1. The spectra of the input synchrotron and bremsstrahlung photons and the resulting spectrum after Comptonization for $a = 0.9$. The resulting spectrum is shown as a solid line. Synchrotron input (*left*) and bremsstrahlung (*right*) use dotted lines.

The Comptonized spectra of synchrotron radiation are smooth enough to allow a power law fit with power index Γ (i.e. $L_\nu \sim \nu^{-\Gamma}$). The fit is not valid at the vicinity of the first peak, which is due to the seed photons. In Fig. 2 we show synchrotron spectra with fits. As can be seen in the plots the slopes of the spectra depend on the model. Since the black hole mass and the accretion rate are the same for all three cases, the differences must be attributed to the black hole angular momentum and its influence on the flow structure. The power law indices estimated from fits are $\Gamma = 0.89, 0.85$, and 0.81 for $a = 0., 0.5$, and 0.9 respectively.

The three spectra resulting from combined effects of synchrotron and bremsstrahlung emission with Comptonization are shown in Fig. 3.

We have also checked the dependence of the observed total luminosity of our models on the observer's position. For the bremsstrahlung photons the dependence is absent. The synchrotron radiation observed from the equatorial plane is stronger by 10 to 20% as compared to the measurement from the axis of rotation.

Following the photons we are able to find the fraction which goes under the horizon. For the synchrotron photons the numbers are: $0.07, 0.05$, and 0.04 for $a = 0, 0.5$ and 0.9 respectively. The bremsstrahlung photons are emitted at relatively larger distances from the horizon and less than 1% of them are lost in all cases. The fraction of photons emitted by the fluid and going under the horizon is a decreasing function of the black hole angular momentum according to our simulations. We have checked this result of our simulations making an independent calculation.

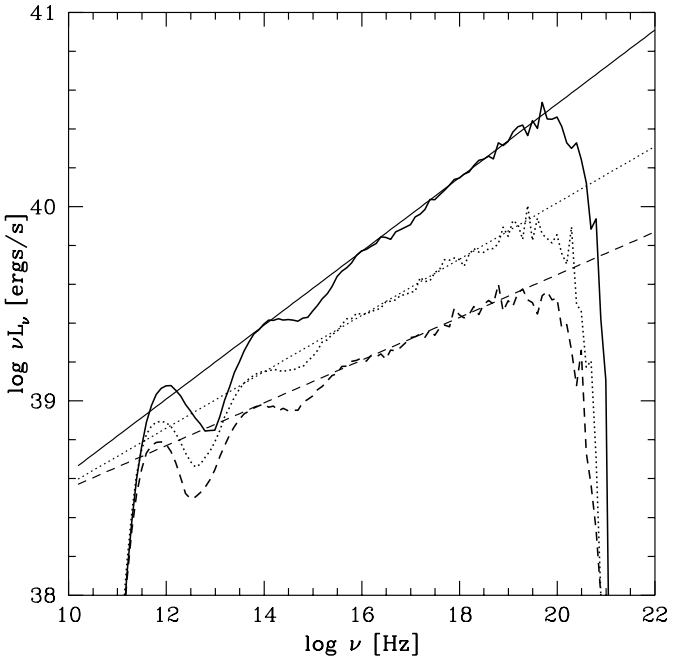

Fig. 2. The power law fits to the Comptonized synchrotron emission for models with black hole angular momentum $a = 0$ (dashed lines), $a = 0.5$ (dotted) and $a = 0.9$ (solid). The corresponding straight lines represent the fits.

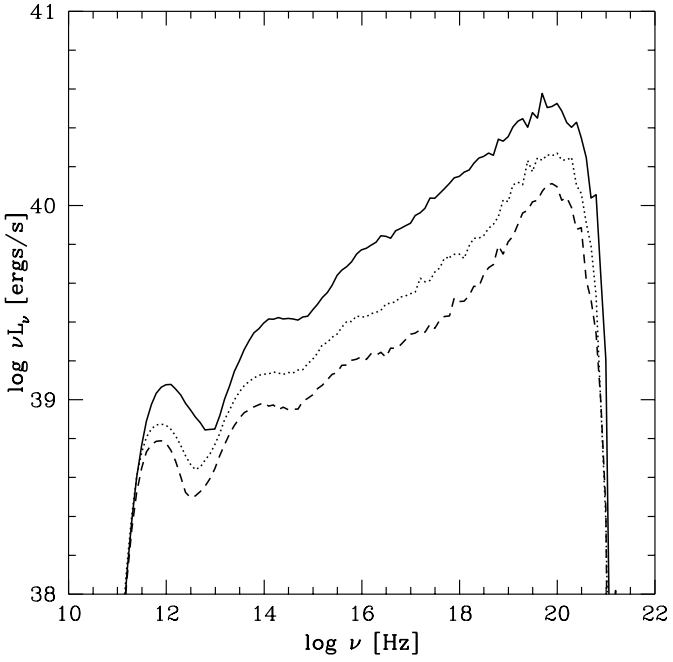

Fig. 3. The resulting spectra of ADAFs for the three cases including the bremsstrahlung component. The conventions follow Fig. 2

We have compared isotropic sources of radiation at the same distance from the black hole, comoving with the matter of the three models we use. Again the fraction of rays going under the horizon is the smallest for the case of the most rapidly rotating hole. The effect must be attributed to the differences in matter kinematics between the three models.

5. Discussion and conclusions

We use the ADAF models from Paper I, but we apply some changes to the treatment of the 3D structure of the flow. The models are still based on vertically averaged, stationary equations for the radial structure of the flow, which uses the vertical scale height and quantities measured at the equator as flow variables. Such treatment can be inadequate near the flow boundary, especially close to the rotation axis. We assume the specific angular momentum of matter, its radial velocity, and the sound speed to be constant on spheres. Under such assumptions it is possible to introduce an effective potential on each sphere, which acts as infinite centrifugal potential barrier near the rotation axis. This infinite barrier causes the sharp drop to zero of matter density there despite the fact that the gas is approximately isothermal on spheres; it effectively removes matter with artificially high angular velocity.

Our models are based on the assumption that all the heat dissipated in the flow goes into the ions. We neglect the direct viscous heating of electrons and the fact that their entropy changes as they fall toward the black hole, which represents the advection of heat. Both mechanisms influence the energy balance equation and, as shown by Nakamura et al. (1997), Narayan et al. (1998) and Quataert & Narayan (1998), have an impact on the electron temperature and the resulting spectrum of the model. While advection of heat by electrons is a well defined process, the viscous heating must be introduced using another free parameter. The combined effects of viscosity and advection on electrons would influence all our models in a similar way, not greatly changing the differences between them.

In our calculations we use three models of the matter flow onto the black hole, with the same accretion rate and the same black hole mass, but with different black hole angular momentum. The spin of the black hole has strong influence on the density and temperature of the matter near the horizon, which are both increasing functions of the rotation rate. Similar behavior of the gas parameters can also be seen in much broader investigation of ADAFs parameter space by Popham & Gammie (1998). We are not able to present a full discussion of the ADAF structure-spectrum dependence, but we can point out some trends.

Our calculations show a strong dependence of the ADAFs spectra on the flow structure resulting from the differences in the black hole angular momentum. The synchrotron seed photons are produced mainly in the central parts of the flow, which are the densest and the hottest. The total energy emitted as synchrotron photons increases with the black hole angular momentum. Also the influence of Comptonization is increased the same way. In the case of $a = 0.9$ model, the Comptonized synchrotron radiation dominates all the way to the highest frequencies, making the usual bremsstrahlung peak invisible. For other cases considered ($a = 0.5$ or 0) this is not true and the bremsstrahlung components dominate at highest frequencies.

The standard theory of Comptonization (Rybicki & Lightman 1979) enables one to estimate the spectral index of low energy radiation, which undergoes multiple scatterings with

thermal relativistic electrons of given temperature and optical depth. In our case both parameters can be defined as averages over the configuration. We have tried several simple prescriptions for calculating the averages, but we have not obtained a quantitative agreement between our results and the estimates, the calculated spectra having spectral indexes by ≈ 0.1 higher (i.e. being steeper). The discrepancies must be attributed to the complexity of the flow and effects such as the relative motion of the starting point of a photon and the place of its interaction with the electrons.

We are not attempting to model NGC 4258, but using the parameters from the model of Lasota et al. (1996) we get the right luminosity in the X-rays for the $a = 0.9$ model. The slope of the calculated spectrum at this frequency (10^{18} Hz) is within the observational bounds. The spectrum of NGC 4258 has been also modeled by Gammie et al. (1998). Although they use slightly different values of the ADAF parameters, their results are very similar to those of Lasota et al. (1996).

Acknowledgements. This work was supported in part by the Polish State Committee for Scientific Research grant 2-P03D-012-12

References

Abramowicz M.A., Chen X., Granath M., Lasota J.-P., 1996, ApJ 471, 762 (ACGL)
Abramowicz M.A., Czerny B., Lasota J.-P., Szuszkiewicz E., 1988, ApJ 332, 646
Abramowicz M.A., Jaroszyński M., Sikora M., 1978, A&A 63, 221
Abramowicz M.A., Lanza A., Percival M.J., 1997, ApJ 479, 179
Akhiezer A.J. Berestetski V.B., 1965, In: Quantum Electrodynamics. Interscience Publications, New York
Balbus S.A., Gammie C.F., Hawley J.F., 1995, ApJ 440, 742
Bardeen J.M., 1973. In: DeWitt C., DeWitt B.S. (eds.) Black Holes. Gordon & Breach, New York, p. 215
Berestetski V.B., Lifshitz E.M., Pitaevski L.P., 1972, In: Relativistic Quantum Theory. Pergamon Press, Oxford
Björnsson G., Abramowicz M.A., Chen X., Lasota J.-P., 1996, ApJ 467, 99
Esin A.A., Narayan R., Ostriker E., Yi I., 1996, ApJ 465, 312
Gammie C.F., Narayan R., Blandford R., 1998, astro-ph/9808036
Gammie C.F., Popham R.G., 1998, ApJ 498, 313
Górecki A., Wilczewski W., 1984, Acta Astron. 34, 141
Jaroszyński M., Kurpiewski A., 1997, A&A 326, 419 (Paper I)
Kato S., Fukue J., Mineshige S., 1998, Black Hole Accretion Disks. Kyoto University Press, Kyoto
Kusunose M., Mineshige S., 1996, ApJ 468, 330
Lasota J.-P., 1994, In: Duschl W.J., Frank J., Meyer F., Meyer-Hoffmeister E., Tscharnuter W.M. (eds.) Theory of the Accretion Disks 2. Kluwer Academic Publishers, Dordrecht, p. 341
Lasota J.-P., 1998, astro-ph/9806064
Lasota J.-P., Abramowicz M.A., Chen X., et al., 1996, ApJ 462, 142
Mahadevan R., 1997, ApJ 477, 585
Mahadevan R., Narayan R., Yi I., 1996, ApJ 465,327
Nakamura K.E., Kusunose M., Matsumoto R., Kato S., 1997, PASJ 49, 503
Narayan R., Barret D., McClintock J.E., 1997, ApJ 482, 448
Narayan R., Mahadevan R., Grindlay J.E., Popham R.G. Gammie, Ch., 1998, ApJ 492, 554
Narayan R., Mahadevan R., Quataert E., 1998, In: Abramowicz M.A., Björnsson G., Pringle J. (eds.) The Theory of Black Hole Accretion Disks. Cambridge University Press, Cambridge
Narayan R., Yi I., 1994, ApJ 428, L13
Pacholczyk A.G., 1970, Radio Astrophysics. Freeman, San Francisco
Peitz J., Appl S., 1997, MNRAS 286, 681
Popham R.G., Gammie C.F., 1998, ApJ 504, 419
Poutanen J., Svensson R., 1996, ApJ 470, 249
Pozdnyakov L.A., Sobol J.M. Sunyaev R.A., 1977, Sov. Astron.-AJ 21, 708
Quataert E., Narayan R., 1998, astro-ph/9810117
Rybicki G., Lightman A., 1979, Radiative Processes in Astrophysics. John Wiley & Sons, Inc., New York
Stepney S., Guilbert P.W., 1983, ApJ 204, 1269
Svensson R., 1982, ApJ 258, 335